Research Paper

Antitumor therapeutic application of self-assembled RNAi-AuNP nanoconstructs: Combination of VEGF-RNAi and photothermal ablation

Sejin Son[1], Namho Kim[1], Dong Gil You, Hong Yeol Yoon, Ji Young Yhee, Kwangmeyung Kim, Ick Chan Kwon✉, Sun Hwa Kim✉

Center for Theragnosis, Biomedical Research Institute, Korea Institute of Science and Technology (KIST), Hwarangno 14-gil 6, Seongbuk-gu, Seoul 136-791, Republic of Korea.

[1]These authors contributed equally.

✉ Corresponding author: Phone: +82-2-958-6639; Email: sunkim@kist.re.kr. Dong Gil You, School of Chemical Engineering, Sungkyunkwan University, Suwon 440-746, Republic of Korea or Dr. Ick Chan Kwon, KU-KIST School, Korea University, 1 Anam-dong, Seongbuk-gu, Seoul 136-701, Republic of Korea

Abstract

Nucleic acid-directed self-assembly provides an attractive method to fabricate prerequisite nanoscale structures for a wide range of technological applications due to the remarkable programmability of DNA/RNA molecules. In this study, exquisite RNAi-AuNP nanoconstructs with various geometries were developed by utilizing anti-VEGF siRNA molecules as RNAi-based therapeutics in addition to their role as building blocks for programmed self-assembly. In particular, the anti-VEGF siRNA-functionalized AuNP nanoconstructs can take additional advantage of gold-nanoclusters for photothermal cancer therapeutic agent. A noticeable technical aspect of self-assembled RNAi-AuNP nanoconstructs in this study is the precise conjugation and separation of designated numbers of therapeutic siRNA onto AuNP to develop highly sophisticated RNA-based building blocks capable of creating various geometries of RNAi-AuNP nano-assemblies. The therapeutic potential of RNAi-AuNP nanoconstructs was validated *in vivo* as well as *in vitro* by combining heat generation capability of AuNP and anti-angiogenesis mechanism of siRNA. This strategy of combining anti-VEGF mechanism for depleting angiogenesis process at initial tumor progression and complete ablation of residual tumors with photothermal activity of AuNP at later tumor stage showed effective tumor growth inhibition and tumor ablation with PC-3 tumor bearing mice.

Key words: small interfering ribonucleic acid (siRNA), gold nanoparticle (AuNP), photothermal therapy, anti-VEGF therapy, combination therapy

Introduction

One ultimate goal of nanotechnology is the construction of more exquisite and robust molecular nanoscale assemblies which are inspired by molecular machinery. In this context, nucleic acids can be seen as an ideal biopolymer for construction of such nanoscale assemblies [1, 2]. Nucleic acids provide remarkable programmability, versatility, and specificity that originate from its composition in addition to the structural and physicochemical properties. These special characteristics arise due to the varying composition and order of four different nucleotide subunits in DNA sequences; adenine (A), cytosine (C), guanine (G), and thymine (T). Predictable and sequence-dependent structure formation is mediated by hybridization between complementary nucleic acid base-pairing, allowing construction of programmable self-assemblies and combination of multiple functional units on a single

nano-assembly with high precision [3-5]. Most of all, the unique and remarkable physiochemical properties of nucleic acids resulting from its chemical composition has provided a basis for rational design of materials with programmable size, shape, and function.

Nucleic acids such as small interfering ribonucleic acid (siRNA), antisense oligonucleotides and micro ribonucleic acid (miRNA) have been regarded as promising therapeutic agents [6-8]. Given the capabilities of high specificity and universal therapeutic targeting, nucleic acids have been consistently demonstrated to be efficacious drugs, and hold high potential in the future of medicine [9-12]. In addition to being therapeutic agents, there has been a recent approach to utilize nucleic acids as highly efficacious biopolymers such as building blocks to assemble sophisticated and biocompatible nano-assemblies [13, 14]. Alongside this approach, through integration of inorganic nano-materials with nucleic acids to obtain biologically beneficial functions, biomedical benefits will be strengthened by nucleic acids mediated self-assemblies such as coupled plasmons and hyperthermia by gold nanoparticles (AuNPs) [15-17]. For example, nucleic acid-modified AuNPs technique was made famous by Chad Mirkin's break-through studies [18]. After that, among various inorganic nanoparticles AuNPs are serving as one of the most attractive materials for nucleic acid delivery applications [15, 19, 20]. One of noticeable examples of these approach is a photothermal therapeutic application by utilizing AuNPs as a heat source as a result of efficient heat generation coming from strong absorption at far-red and near infrared (NIR) wavelengths [21-23]. Therefore, more recent efforts have focused on constructing sophisticated AuNP and nucleic acid hybrid nano-assemblies engineered with great precision [15, 22]. Most attempts have been concentrated on studying the dynamics or programmed behaviors of nano-assembly itself, especially the transition between two different configurations of the NPs translating into dynamic motion for switching on or off [24, 25]. Despite, the therapeutic usefulness of hybrid nucleic acids based AuNPs should not be overlooked in terms of therapeutic potentials of nucleic acids, although their physical aspects themselves are very attractive and promising. Therefore, in this study, hybrid RNA-based AuNP nanoconstructs were paid attention not only as a sophisticated nano-assembly but also as a therapeutic reagent.

In this study, we present a platform technology to construct sophisticated hybrid RNA-based AuNP nanoscale assemblies (RNAi-AuNP) which can function as both effective building blocks for programmed nanoconstructs and photothermal therapeutic agents for treating tumors (Fig. 1). First, we performed precise conjugations of designated numbers of RNA onto AuNP followed by specific separation of each AuNP with individual numbers of RNA to provide building blocks that are highly effective and capable of creating various geometries of RNAi-AuNP nano-assemblies through complimentary base-pairing between RNAi-AuNP building blocks. Although gold nanostructures may have potential for photothermal therapy (PTT), small-sized RNAi-AuNPs alone is a suboptimal formulation for *in vivo* applications due to their absorbance wavelength lying in the visible spectral range [21]. Herein, the condensed and compact nanocluster form of PEI/RNAi-AuNP complexes was utilized for further studies of their photothermal ablation *in vitro* and *in vivo*. More importantly, beneficial biological functions such as RNAi mechanisms and photothermal therapeutic function could be integrated together for anti-tumor therapeutic application.

Materials and Methods

Materials

Gold nanoparticles (AuNP) were purchased from BBI Solutions (Cardiff, UK). siRNA and oligonucleotides were synthesized by and purchased from Integrated DNA Technologies (Coralville, USA) and Bioneer Co. (Daejeon, South Korea). Branched Polyethylenimine (MW 25,000, BPEI), dithiothreitol (DTT), 11-mercaptoundecanoic acid (MUA), and all cell culture reagents were purchased from Sigma-Aldrich (St. Louis, USA). Opti-MEM was purchased from Thermo Fisher Scientific (Waltham, MA, USA). Amicon MWCO centrifugal filter units were purchased from Merck Millipore (Darmstadt, Germany). 8 kDa MWCO dialysis tubing was purchased from SpectrumLab (USA).

Conjugation of designated numbers of DNA/RNA onto AuNP

Before DNA or siRNA conjugation onto AuNP, AuNP's surface was stabilized with MUA. The pH of AuNP was adjusted to 11 by slow addition of 1 M NaOH. 50 mg of MUA was dissolved in 1 ml of 100% ethanol. The MUA solution was added drop-wise to a final concentration of 0.1 mg/ml in 500 ml of 3.21×10^{-4} M AuNP solution, and stirred overnight at room temperature. Residual MUA was eliminated by centrifugation with Amicon 30kDa MWCO centrifugal filter units, washing five times with deionized water and 70% ethanol. Sense and

anti-sense strands of siRNA bearing thiol groups at the 5′-ends were dissolved separately in 500 µl of Tris/Borate/EDTA (TBE) buffer. Dithiothreitol (DTT) was added at final concentration of 20 mM and each sample was incubated at 37 °C for 1 h to activate the thiol groups for further process. The siRNAs were then purified using PD Minitrap G-25 columns (GE Healthcare) by size exclusion method to remove DTT and by product. The concentration of each thiol activated siRNA sample was quantified by using the Beer-Lambert law (absorbance=εcl). The absorbance at 260 nm wavelength was measured with BioPhotometer Plus (Eppendorf). MUA coated AuNPs and each type of thiol activated siRNA or DNA strands were mixed at 1:1 molar ratio to prepare AuNPs with designated numbers (n) of DNA/RNA (DNA/RNA-n-AuNP) in presence of 50 mM NaCl for 2 h at room temperature. The DNA/RNA-n-AuNP were then purified with 100 mM NaCl/0.5X TBE buffer several times by centrifugation at 13,200 rpm for 1~2 min at 4 °C by using 10 kDa MWCO filter units.

Separation and extraction of DNA/RNA-n-AuNP

After purification, each DNA/RNA-n-AuNP were separated in 2% agarose gel by electrophoresis. Each well of the agarose gel was loaded with approximately 100 pmol of DNA/RNA-n-AuNP and was run for 30 min at 100V. Each band was cut with a razor blade and put into an 8 kDa MWCO dialysis membrane, then was put back into the gel electrophoresis apparatus to extract each DNA/RNA-n-AuNP out from the gel fragment at 18V for 40 min.

Annealing of complementary DNA/RNA-n-AuNP

For constructing complementary nucleic acid-mediated AuNP assemblies, the mixture of AuNPs with complementary DNAs or antisense- and sense- RNAs were annealed by heating up the mixture to 95 °C for 2 min and slowly cooling down to room temperature for 1 h. To confirm the hybridization of nucleic acids of AuNPs, UV/VIS absorbance spectrum was monitored and concentration was quantified by measuring AuNP absorbance at 520 nm wavelength with UV-VIS.

Preparation and characterization of PEI/RNAi-AuNP complexes

RNAi-AuNPs were formulated with cationic reducible branched PEI in order to be delivered into cells effectively (PEI/RNAi-AuNP). PEI/RNAi-AuNP complexes were prepared at various nitrogen of PEI to phosphates of nucleic acids (N/P) ratios from 1 to 50 by adding the 0.1 mg/ml PEI solution to the RNAi-AuNP solution in DPBS buffer (pH 7.4). The mixture was incubated for 15 min at room temperature to allow nanoparticle formation. The hydrodynamic diameter of each formulation was measured in distilled water by using Zetasizer Nano S (Malvern Instruments, Malvern, UK). The morphology was observed using transmission electron microscope (TEM, Phillips CM30) at an accelerating voltage of 200 ekV. For TEM images, samples were diluted in deionized water by 500-fold and dropped on 200-mesh copper grids.

Cellular Uptake

2×10^5 PC-3 cells were seeded on glass-bottom 35mm dishes. After overnight incubation, cells were exposed to 2 µg of PEI/RNAi-AuNP for 3 h. Intracellular uptake of PEI/RNAi-AuNP was visualized with fluorescence microscope (1X81, Olympus, Tokyo, Japan) equipped with a dark field condenser. For dark-field imaging, coverslips were fixed using 4% formaldehyde and mounted on slide glass with an aqueous mounting media with an anti-fading agent (Vector Laboratories Inc., Burlingame, CA).

In vitro gene knockdown experiments

In order to confirm VEGF gene knockdown efficiency (5′-GGAGUACCCUGAUGAGAUCdTdT-3′, 5′-GAUCUCAUCAGGGUACCCdTdT-3′), PC-3 cells were cultured in RPMI 1640 media supplemented with 10% fetal bovine serum (FBS) and 1% antibiotics. 2×10^5 PC-3 cells were seeded in each well of 6-well plates and incubated overnight. After changing media to 1.5 ml of Opti-MEM, each formulation was treated to each well at 4ug siRNA/well. All experiments were done in triplicates. All PEI/RNAi-AuNP complexes were formed at N/P ratio of 30 in Dulbecco's phosphate buffered saline (DPBS) for 15 min at room temperature, as mentioned above. After 4 h incubation, each well was refreshed with the growth media. For quantification of VEGF protein level, the media was harvested after 24, 48, and 72 h. VEGF level was quantified by using Quantikine Human VEGF Immunoassay kit (R&D Systems, Minnesota, USA) according to the manufacturer's protocol.

Cytotoxicity

PC-3 cells were seeded in a 96-well plate at a density of 6×10^3 cells per well, and were incubated overnight at 37°C/5% CO_2 humidified environment in RPMI medium supplemented with 10% (v/v) FBS and 1% (v/v) anti-biotics. Various amounts of PEI/RNAi-AuNP complexes at N/P ratio of 30 were

added to the wells and were incubated overnight. Cytotoxicity of our siVEGF sequence was comparatively analyzed with CCK-8 (Dojindo Molecular Technologies), following the manufacturer's protocol.

In vitro photothermal effect of PEI/RNAi-AuNP

PC-3 cells were seeded in a 48-well plate at a density of 1×10^6 cells per well and were incubated overnight. Cells were treated with varying amount of PEI/RNAi-AuNP to confirm that photothermal therapeutic effect is in dose-dependent manner. After incubation for 3 h and washing with RPMI1640, each well was exposed to CW diode laser (655nm) for 4 min. After incubation for 45 min, cells were stained with 50% trypan blue for 10 min to observe cell viability through microscope.

Experimental settings of HIFU system

Animal HIFU system (VIFU 2000, Alpinion, Korea) was used for *in vivo* experiments. The mice were fixed on the holder for treatment. The water bath was maintained at 37 °C and degassed by the automatic VIFU 2000 system. The *in vivo* temperature was measured using a thermocouple wire (50 μm in diameter, Physitemp Instrument Inc., Clifton, NJ) inserted into the tumor tissue.

In vivo antitumor therapeutic efficacy

All experiments with live animals were performed in compliance with the relevant laws and institutional guidelines of Korea Institute of Science and Technology (KIST). The antitumor efficacy of PEI/RNAi-AuNP complexes was determined by measuring tumor volume for 30 days. 5-week-old Balb/c nude mice (purchased from Orient Bio, Sungnam, Korea) were injected subcutaneously in the left flank with PC-3 cells. When tumor reached a volume of 100 mm³, mice were divided into six groups: (a) saline, (b) saline + laser, (C) saline + HIFU, (d) PEI/RNAi-AuNP, (e) PEI/RNAi-AuNP + laser, and (f) PEI/RNAi-AuNP + HIFU (n = 4 per each group). Basically, all formulations were directly delivered through multiple intratumoral injections to alleviate the serum stability concerns of PEI/RNAi-AuNP having a strong positive surface charge. Intratumoral injections of PEI/RNAi-AuNP were administered every 3 days. After total injection of PEI/RNAi-AuNP, the mice were treated by 655nm CW laser or HIFU (power: 50 W, frequency: 1.5 MHz, duty cycle: 10 %, pulse repetition frequency: 1 Hz, time: 30 sec, interval: 1 mm). The tumor site was completely exposed to laser or HIFU. The treatment of laser or HIFU was conducted once every 3 days. Total

treatment of laser or HIFU was 3 times. Tumor volumes were calculated as $\mathbf{a} \times \mathbf{b}^2 \times 0.54$, where $\mathbf{a}$ was the largest and $\mathbf{b}$ was the smallest diameter. The tumor growth images were obtained using small imaging system (OV-100, Olympus, Center Valley, PA) in bright field.

### Statistics

Data was analyzed with one-way ANOVA with appropriate post hoc test for multiple group comparison. Unpaired student's t-test was also done for comparison between two groups as shown in figure legends. The values of $p < 0.05$ were considered statistically significant.

Results and Discussion

Preparation of AuNP conjugates with designated numbers of nucleic acids

The main idea and experimental concept of this study is the conjugation and separation of DNA/RNA-AuNP conjugates with n-designated numbers of single stranded DNA or RNA denoted as DNA-n-AuNP or RNA-n-AuNP (n=1, 2, 3, 4, 5) to construct versatile, therapeutic RNA-AuNP nano-assemblies. The conjugation of different numbers of nucleic acid strands and separation of each DNA/RNA-n-AuNP provided the building blocks to construct various geometries of DNA/RNA-AuNP nano-assemblies. This process is mediated by the spontaneous and programmed self-assembly formation between complementary base-pairs of DNA or RNA sequences attached to AuNPs as illustrated in Figure 1. The main challenge in preparation of DNA/RNA-n-AuNP conjugates is that AuNPs are prone to forming aggregates in various buffer environments during both preparation and purification processes. Thus, it is important to stabilize the AuNP surface for multiple formulation processes such as electrophoresis, annealing, and purification. AuNPs were stabilized by 11-mercaptoundecanoic acid (MUA) to prevent AuNPs from forming large aggregates in various buffers and under the harsh conditions of electrophoresis before DNA and RNA strands are conjugated onto the AuNP surface. The hydrodynamic data showed a slight increase in size from 5 nm to 7 nm after MUA modification (Fig. 2a). There was no UV-VIS spectrum change as the maximum resonance in absorption was 519 nm before and after MUA modification (Fig. 2b), which indicates that MUA modification does not change the resonance property of AuNPs.
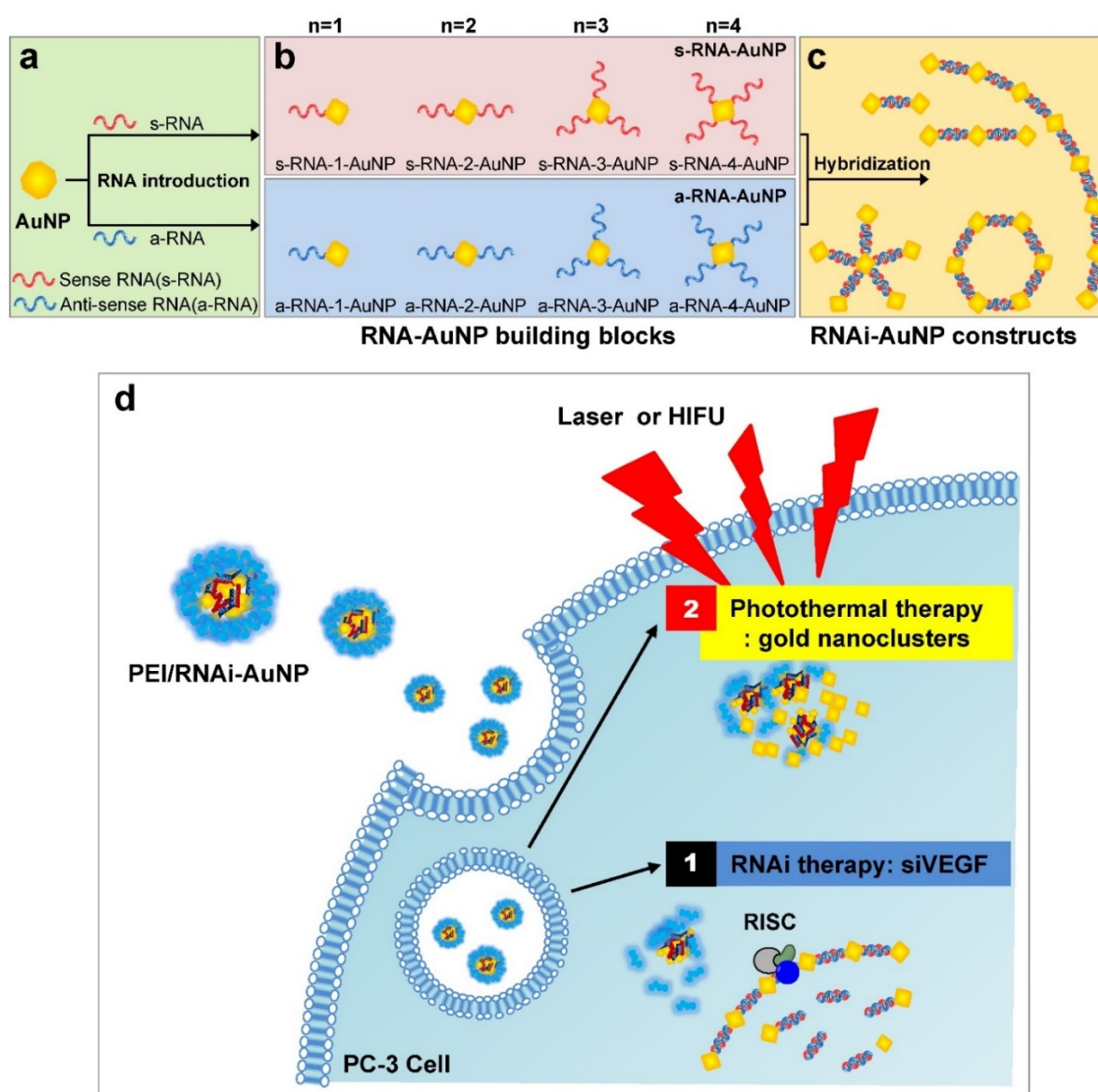
Figure 1. Schematic illustration of RNAi-AuNPs with various geometries constructed by programmed self-assembly formation between complementary base fairing between antisense and sense-RNA strands. RNA conjugated AuNP with n-designated numbers of RNA strands were produced by (a) thiol-ligand chemistry as (b) highly sophisticated building blocks to assemble (c) versatile RNAi-AuNP hybrid nanoconstructs. (d) Schematic illustration of a combinational strategy of anti-angiogenesis mechanisms and photothermal ablation to maximize anti-tumoral therapeutic efficacy. Anti-angiogenesis therapy with anti-VEGF siRNA to reduce tumor growth was performed on early tumor progress and photothermal therapy was sequentially followed to eradicate cancer completely at later stages of tumor development.

For the preparation of DNA-n-AuNP, designated numbers of DNA strands on each MUA-AuNP were mixed at 1:1 molar ratio for 2 hr. As a model system for RNA-AuNP, 80 bases-long deoxynucleotides of poly(deoxyadenine) denoted as poly(dA) and poly(deoxythymidines) denoted as poly(dT) were chosen as complementary DNA strands to serve as building blocks to assemble various DNA-AuNP nano-assemblies. For clear separations of each AuNP with designated n-DNAs, the diameters of AuNP as well as the lengths of DNA were considered carefully. When the DNA or RNA is attached to a gold nanoparticle, the separation ability is highly dependent on the size of the gold

nanoparticles. Therefore, smaller diameter of AuNP and longer length of DNA led to easier and more prominent separation of each DNA-n-AuNP on agarose gel (data not shown) [26, 27]. Therefore, 5 nm diameter of AuNP and 80 bases-long poly(dA) and poly(dT) strands were chosen for effective separation and purification. After conjugation of poly(dA) and poly(dT) strands on AuNP, each DNA-n-AuNP was separated on 2% agarose gel depending on the numbers of DNA strands on the AuNP. As a result, poly(dT)-n-AuNP showed clear separation on the gel, showing single bands of each poly(dT)-n-AuNP from n=1 to n=5 (Fig. 1c). The DNA-n-AuNP mixture can be effectively separated by charge and/or length of

DNA fragment in the agarose gel matrix if the size of AuNP is small enough. Specifically, poly(dT)-1-AuNP migrated the farthest from the starting point (top of the agarose gel) while poly(dT)-5-AuNP remained the closest. On the other hand, for poly(dA)-n-AuNP, incomplete separation was observed on the agarose gel matrix although discrete bands were distinguishable for each number of poly(dA) on AuNP given that the trailing red bands were seen on the agarose gel. This behavior of poly(dA)-n-AuNP may be explained by poly(dA)'s high affinity for AuNP surface [28], supporting that poly(dA) strands can physically interact with AuNP surface by still elusive noncovalent interaction as well as 5'-thiol covalent conjugation of poly(dA) to AuNP's surface [29, 30].

For therapeutic application, sense and anti-sense RNA strands containing siRNA sequence for vascular endothelial growth factor (VEGF) were conjugated on AuNP via 5'-thiol-mediated conjugation. Each anti-sense and sense VEGF-RNA strand, denoted as a-RNA and s-RNA, respectively, were synthesized as complementary building blocks to construct therapeutic RNA-AuNPs (Fig. 1 a,b). Three repeated sequences of anti-sense or sense VEGF siRNA were connected by 4-base paired DNA spacer (-ATGC- for sense strand, -GCAT- for anti-sense strand). After 2 h incubation of both sense and anti-sense RNA strands with MUA-AuNPs to produce a-RNA-n-AuNP and s-RNA-n-AuNP respectively, agarose gel was run to separate them by the number of RNA strands on each AuNP. As a result, separated bands of a-RNA-n-AuNP and s-RNA-n-AuNP were visualized on agarose gel (n=1, 2, 3, and 4) (Fig. 2d). Each a-RNA-n-AuNP and s-RNA-n-AuNP was extracted from each clipped band by electrophoresis to be further processed (Detailed procedure is described in Method).
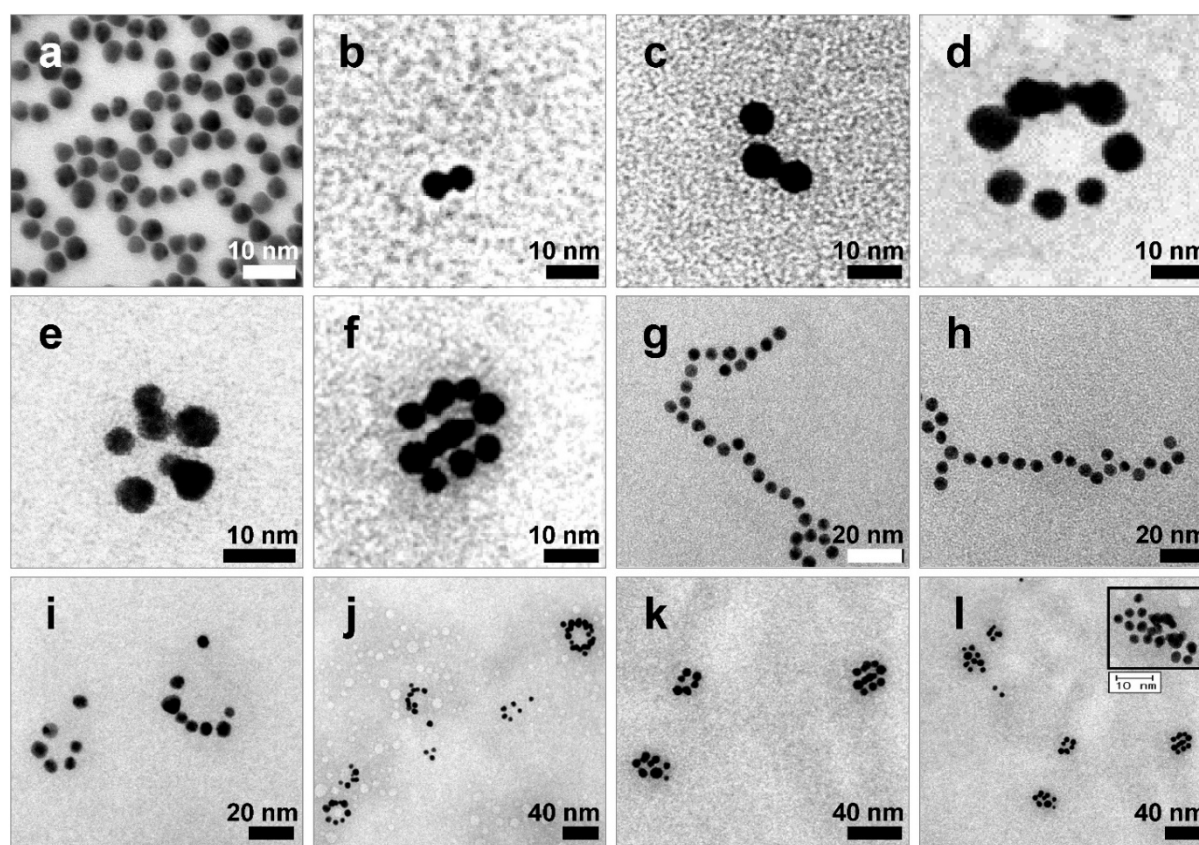
Construction of RNAi-AuNP nanoconstructs with various geometries

After extraction of each s- and a-RNA-n-AuNP from agarose gel, they were mixed together to form various self-assemblies of different geometries via base-pairing between complementary a-RNA and s-RNA strands (Fig. 1c). Depending on the number of RNA strands introduced onto the AuNPs, various geometries of RNAi-AuNP nano-assemblies were achieved. TEM images showed the varying geometries of RNAi-AuNP nano-assemblies (Fig. 3): the a-RNA-AuNP and s-RNA-AuNP with only a single RNA strand resulted in dumbbell-like nanostructures (Fig. 3b and c), the AuNP mixture with double and triple strands of RNA led to the formation of ring and spherical AuNP nano-structures (Fig. 3d, e, f, i, j, k, and l), and long and stretched poly(RNAi-AuNP) nanostructures were also constructed (Fig. 3g and h). On average, 20 AuNPs were connected to each other by complementary base-pairing between the a- and s-RNA strands of AuNP by manually counting them based on TEM images. Hence, a total of approximately 60 VEGF siRNAs could be polymerized per each poly(RNAi-AuNP).
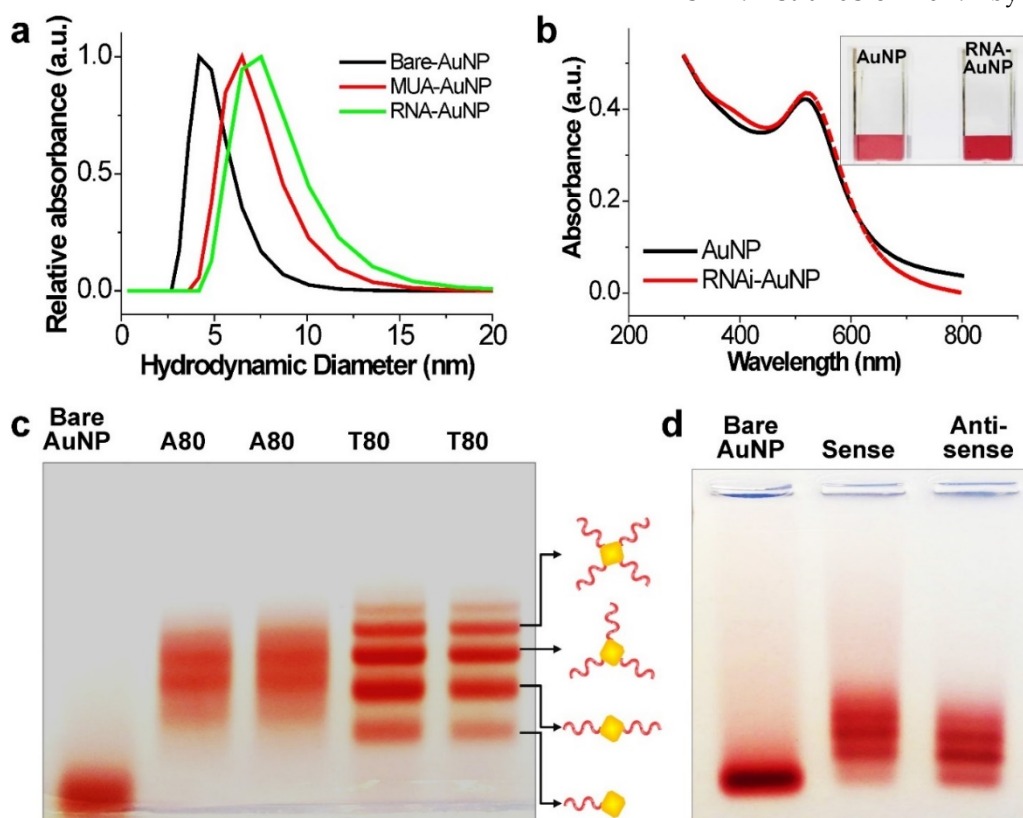
Figure 2. Investigation of effective formulation of RNA/DNA-AuNP. (a) Hydrodynamic sizes of bare-AuNP, MUA-AuNP and RNA-AuNP by DLS and (b) UV-VIS spectrum change before and after RNA conjugation onto AuNP, (c) effective separation of DNA-n-AuNP and (d) a-RNA-n-AuNP and s-RNA-n-RNA on 2% agarose gel depending on the conjugated numbers of DNAs/RNAs on AuNP.

Figure 3. TEM images of RNAi-AuNP nanoconstructs with various geometries assembled by a-RNA-n-AuNP and s-RNA-n-AuNP building blocks. Depending on the numbers of RNA ligands on AuNP, (a) Bare-AuNP, (b, c) Dumbbell-like nanoconstructs with a single RNA ligand on AuNP, (d, e, f, i, j, k and l) ring and spherical AuNP nanoconstructs with double and triple strands of RNA on AuNP and (g, h) long and stretched poly(RNA-AuNP) nanoconstructs were observed.

Preparation and characterization of PEI/RNAi-AuNPs for therapeutic application

For successful therapeutic RNAi, poly(RNAi-AuNP) was chosen as the optimal formulation since it provided the highest therapeutic siRNA loading capacity and efficiently complexed with a cationic agent of branched polyethylenimine (PEI) to form condensed and compact nanoparticles, denoted as PEI/RNAi-AuNP, for effective intracellular delivery (Fig. 1d). At optimal complexation condition of N/P ratio of 30 based on nitrogen (N) numbers in PEI to phosphate (P) numbers in siRNA (Fig. S1a and S1b), PEI/RNAi-AuNP could form small and compact nanoparticles with PEI allowing for intracellular delivery. The resulting hydrodynamic size and zeta potential were ca. 300 nm and + 32 mV, respectively, for PEI/RNAi-AuNP after 15 min incubation with PEI at N/P=30 in DPBS buffer (Fig. 4a). The UV-VIS spectrum of PEI/RNAi-AuNP became wider and the maximum resonance in absorption was shifted from 519 nm to 670 nm (Fig. 4b). The resonance shift to a longer wavelength in absorption is a clear indication of large AuNP aggregates. It is well known that AuNPs present different optical and resonance properties depending on their size; larger and bulkier AuNPs absorb at longer wavelengths than smaller or individual AuNPs [31]. Therefore, this aspect elicits coupled surface plasmons and strong absorption at far-red and near infrared (NIR) wavelengths with efficient heat conversion [15, 21, 22]. More precise observation of AuNPs was carried out through TEM imaging with and without uranyl acetate staining allowing observation of the spherical shape of PEI/RNAi-AuNPs and their precise nanostructure formations. With staining, PEI polymer could be visualized prominently as a lighter region (Fig. 4c) but AuNPs were not seen under TEM since an excess amount of PEI (N/P=30) covered and embraced the AuNP aggregates completely. On the other hand, with small amount of PEI (N/P=1) the AuNP aggregate formation was able to be clearly visualized. Also, when we tried to measure the size of the various geometries of RNAi-AuNPs with PEI complexation, we could not acquire actual size data since they form large aggregates with PEI polymers in water and PBS buffer (data not shown). Additionally, when we observed them by TEM, most had failed to form stabilized and compact nanoparticles unlike PEI/poly(siRNA-AuNP) formulations (Fig. S2).
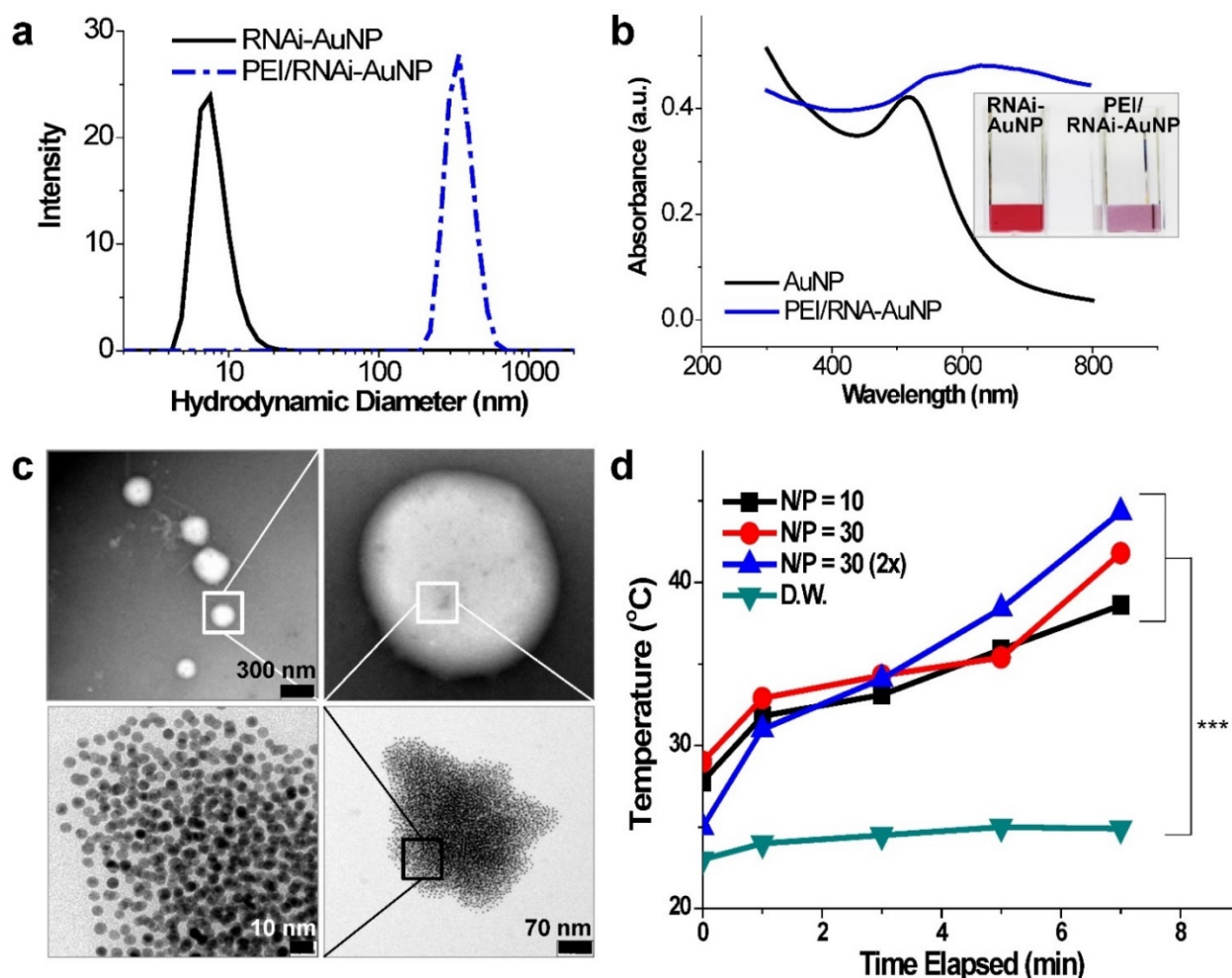
Figure 4. Physicochemical properties of PEI/RNAi-AuNP nanoformulations in terms of (a) hydrodynamic size changes and (b) UV-VIS spectrum changes before and after forming complexes with PEI polymer. (c) TEM images of PEI/RNAi-AuNP in the presence of appropriate amount of PEI (N/P=30 in PBS) forming a compact and condensed nanoparticle structure and (d) with low concentration of PEI (N/P=1 in PBS). (e) The heat generation efficacy of PEI/RNAi-AuNP was monitored by measuring the temperature change of water as CW laser at 655 nm is being irradiated during 7 min. *** $P<0.001$ (n = 3).

In order to verify the potential of using PEI/RNAi-AuNP as a photothermal therapy agent, UV-Vis absorption properties were evaluated. As results, with the exception of PEI/poly(RNAi-AuNP), the complexes of PEI/various geometries of RNAi-AuNPs such as dumbbell, ring, and spherical shapes did not demonstrate suitable UV absorption properties for efficient heat conversion as shown below (Fig. S3). The formulation of RNAi-AuNP ideally should absorb the long wavelengths of far-red and near-infrared (NIR) or at least longer than 650 nm as mentioned above. For further evaluation for photothermal therapeutic agents, the PEI/RNAi-AuNP solutions with different concentrations and N/P ratios were exposed to external CW laser irradiation (655nm) for 7 min (Fig. 4d). The heat generated from the photothermal effects of PEI/RNAi-AuNP was gradually increased with the increase of irradiation time. After 7 min exposure to the laser irradiation, the temperature of the PEI/RNAi-AuNP solutions had reached nearly 40 °C. When the concentration of PEI/RNAi-AuNP at N/P ratio of 30 solutions was doubled, the heat generation efficiency was further enhanced and finally the solution temperature reached over 45 °C after 7 min. Since the threshold temperature required for thermal ablation-induced cell death is around 45 °C [15], the use of PEI/RNAi-AuNP as a photothermal ablation agent seems well worth considering for cancer therapy.

In vitro gene silencing efficiency, cytotoxicity, and photothermal efficacy

The target gene silencing efficacy of PEI/RNAi-AuNP containing anti-VEGF siRNA was confirmed by measuring VEGF protein expression levels of PC-3 cells. Before transfection of PC-3 cells with PEI/RNAi-AuNP, effective intracellular uptake and intracellular release of siRNA were confirmed by dark field microscopic images (Fig. S4). After 6 h incubation, the majority of RNAi-AuNPs were evenly

distributed throughout the cytoplasm of the PC-3 cells indicative of effective intracellular uptake, dissociation and the release of siRNA-AuNPs from PEI/RNAi-AuNP formulation. For PEI/RNAi-AuNP, PEI mainly dictates the surface properties of RNAi-AuNPs such as surface charge and cellular membrane interactions as shown in Fig. 4c [32]. Therefore, the proton sponge effect caused by PEI may result in the endosomal release of PEI/RNAi-AuNPs after effective cellular uptake as same with other PEI based nanoparticles [33] [34]. To examine the VEGF gene silencing efficacy of poly(RNAi-AuNP), PEI/RNAi-AuNPs and PEI/RNAi prepared with varying N/P ratios of 10, 20, and 30 were transfected to PC-3 cells (Fig. 5a,b). The free siRNA trimer-PEI complex formulation without AuNP conjugation (denoted as PEI/RNAi) was considered as a positive control group. Forty-eight hours after siRNA transfection, both PEI/RNAi-AuNP and PEI/RNAi exhibited an increase in VEGF gene silencing efficacy with increasing N/P ratio (Fig. 5a). However, compared to the PEI/RNAi with free siVEGF, PEI/RNAi-AuNP showed quite lower gene silencing activity particularly at low N/P ratios of 10 and 20 due to poor complexation abilities of cationic polymer of PEI with poly(RNAi-AuNP). At lower N/P ratios of 10 and 20 where the incomplete complexation observed (Figure S1), the transfection efficacy was also negligible for PEI/RNAi-AuNP at all tested condition [11,12]. On the contrary, under an optimal formulation condition with N/P=30 in terms of hydrodynamic size and TEM analysis, PEI/RNAi-AuNP showed a significant VEGF gene silencing level (ca. 40% gene silencing). Interestingly, when the transfection period was increased from 48 to 72 h, the gene silencing activity of PEI/RNAi-AuNP was reached to approximately 65% (Fig. 5b). This result indicates that poly(RNAi-AuNP) has somewhat delayed RNAi response due to steric hindrance of bulky AuNPs nanoclusters inside cytosol, compared to free siVEGF trimers without AuNPs. Furthermore, the gene silencing efficacy of siVEGF was highly dependent upon the repeating number of siVEGF sequences as well as incubation time as shown in Fig. S5. At lower numbers of repeating number of siVEGF and longer incubation period, significantly higher gene transfection efficacy was demonstrated. And the gene silencing effect of PEI/RNAi-AuNP was siVEGF sequence specific in the sense of that scrambled PEI/RNAi-AuNP was not present any VEGF protein expression in ELISA (Fig. S6a) and western blotting analysis (Fig. S6b) When the cytotoxic effects of poly(RNAi-AuNP), PEI/RNAi-AuNP, and PEI/RNAi with three different concentrations were evaluated in

PC-3 cells, there was no noticeable cytotoxicity in all tested samples up to 48 h (Fig. 5c).
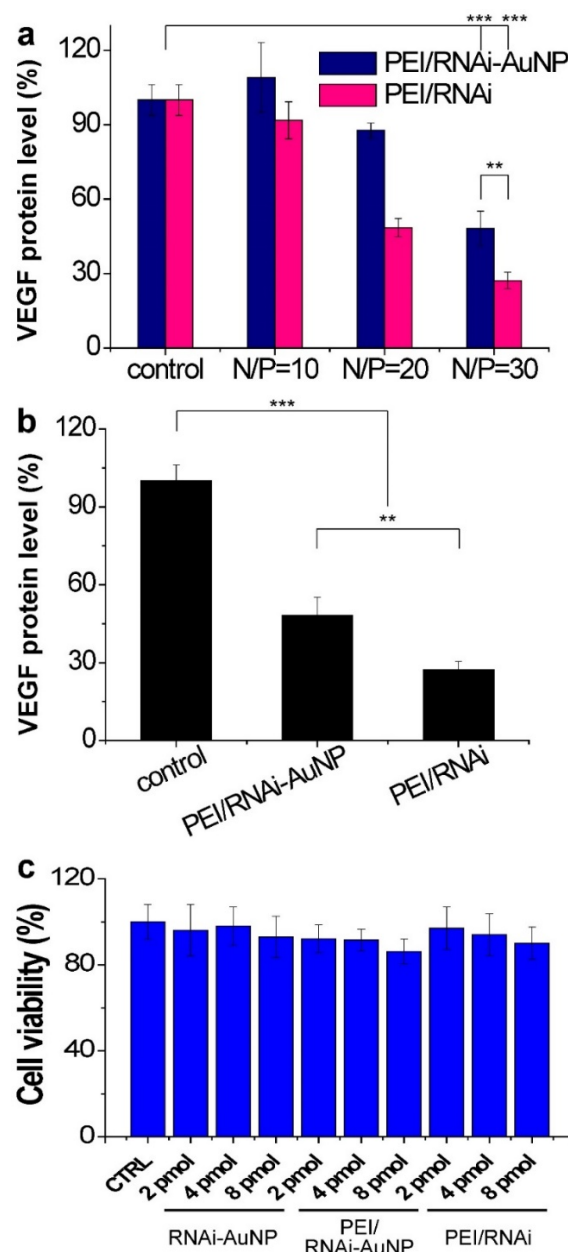

Figure 5. In vitro cell studies of PEI/RNAi-AuNP to validate therapeutic potential. (a) in vitro siVEGF gene silencing efficacy by measuring VEGF protein level after 48 h transfection with varying formulations in comparison with PEI-RNAi complexes without AuNP. (b) Maximized gene silencing efficacy of optimized PEI/RNAi-AuNP (N/P=30) after 72 h transfection. (c) Cytotoxicity study of all formulations in various concentrations. ** P<0.01 and *** P<0.001 (n = 3).

The photothermal effects of PEI/RNAi-AuNP on PC-3 cells were studied with a 655 nm CW diode laser radiation in vitro condition. After 4 h transfection under varying concentrations of PEI/RNAi-AuNPs, the cells were exposed to CW diode laser for 0.5, 2, and 4 min and stained with 50% trypan blue to visualize cell damage and death by the dark blue color

(Fig. 6a). As result, 4 min of laser exposure was enough to induce cancer cell death by NIR radiation and the extent of cell damage was directly proportional to the amount of PEI/RNAi-AuNP in all tested condition. Specifically, at the highest dose (1600 ng/well), only 30 seconds of laser exposure to PC-3 cells imposed severe cell damage and 4 min irradiation led to almost 100% cell death. In contrast, PC-3 cells without PEI/RNAi-AuNP and PEI/RNAi did not show any cell damage after laser irradiation of any duration. This observation clearly demonstrates that the cell damage and death are only induced by the heat generated from PEI/RNAi-AuNP, not laser irradiation itself. The heat generation ability of PEI/RNAi-AuNP under *in vivo* conditions was further verified with PC-3 tumor bearing mice (Fig. 6b). The local temperatures of solid tumors were monitored over a course of time after intratumoral injection of PEI/RNAi-AuNP with varying concentrations. Laser irradiation onto PC-3 tumors of mice treated with PEI/RNAi-AuNP led to a gradual increase in local temperature from 33°C up to 45°C in 10 minutes at all concentrations. Particularly, in the highest particle concentration an abrupt temperature increase to 53°C was observed at 15 min of laser irradiation. These *in vitro* and *in vivo* results associated with photothermal heat generation support that PEI/RNAi-AuNP imposes sufficient therapeutic potential as a photothermal ablation agent for cancer therapy.
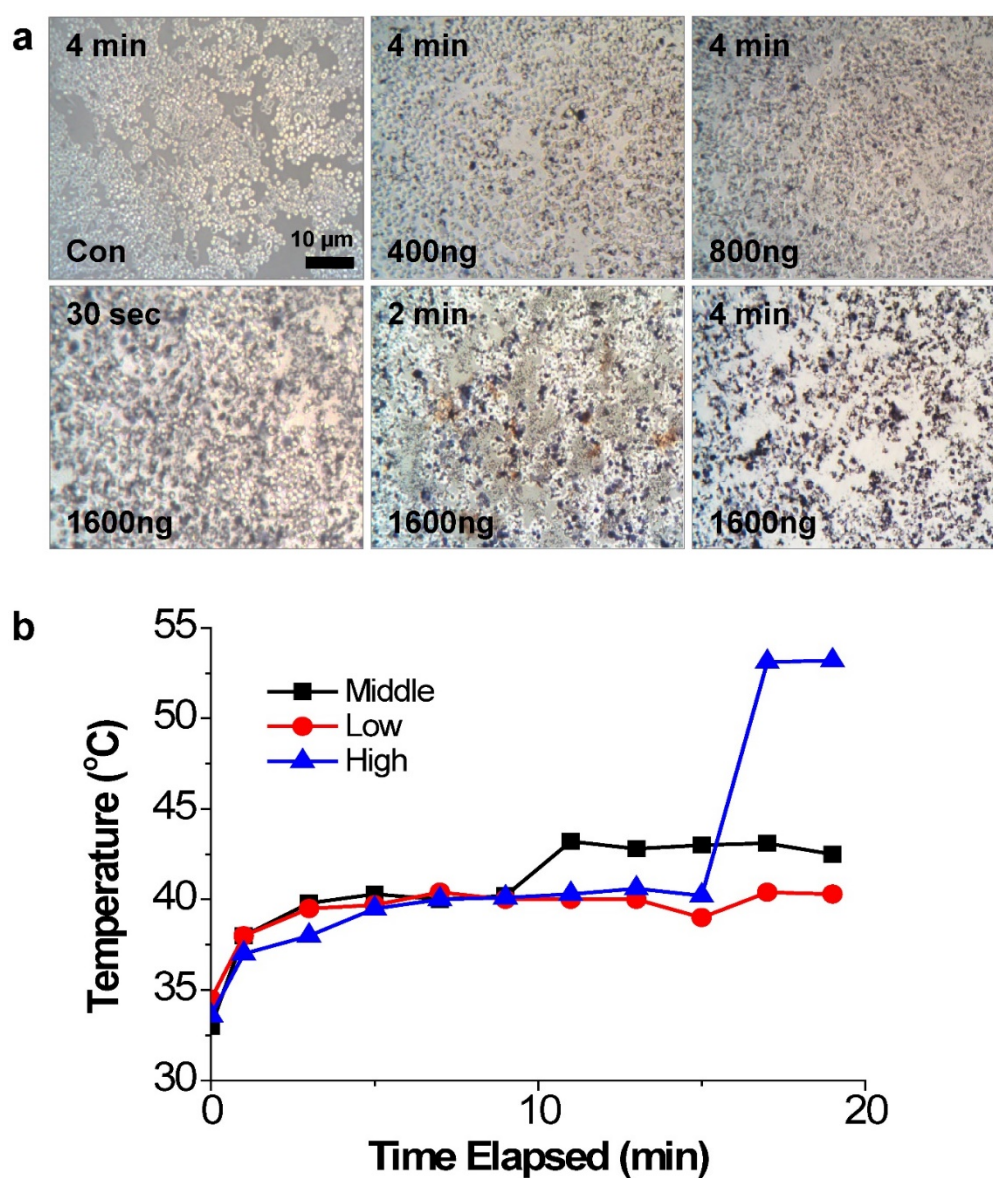
Figure 6. The photothermal effects of PEI/RNAi-AuNP on PC-3 cells with laser irradiation. (a) Damaged and dead cells with varying concentration of PEI/RNAi-AuNP at different time points with 50% trypan blue staining after 4 h of cellular uptake. (b) The local temperature change in PC-3 tumors of mice measured over time post intratumoral injection of PEI/RNAi-AuNP with varying concentration.

Combinational antitumor therapy of PEI/RNAi-AuNP

Up till now, there have been various anti-VEGF targeting approaches for anti-angiogenic cancer therapy. Most current anti-VEGF monotherapies, however, have failed to increase survival rates in many clinical cases. Several recent reports suggest that anti-VEGF therapy alone becomes less effective and meets resistance primarily due to anti-VEGF escape mechanisms of tumors and their heterogeneous microenvironments [35, 36]. Although anti-VEGF monotherapy does not lead to cancer cell death directly, it can obviously attenuate cancer angiogenesis and substantially reduce tumor growth. With these concerns in mind, combination of anti-angiogenesis with photothermal ablation would be a sound strategy for antitumor therapy [37, 38]. Thus, we hypothesized that anti-tumoral therapeutic efficacy would be maximized by a sequential application of anti-VEGF therapy at relatively early stages of tumor progression followed by photothermal ablation in order to overcome the issue of resistance during the later stages in tumor development. In other words, the timing of laser irradiation was carefully chosen by determining the point in time where the tumor growth accelerated thus indicating the slowing down of the VEGF gene silencing activity. At this point in time, the efficacy of the siRNA therapy could be neglected and both treatments can be considered independent of one another from this point forward.

For *in vivo* anti-tumoral therapy, CW lasers or high intensity focused ultrasound (HIFU) was utilized as a tool to activate PEI/RNAi-AuNP for heat generation. HIFU technology has recently appeared as a non-invasive method for tumor ablation [39], since the ultrasound beam can be focused directly to the tumor below the skin surface and generate sufficient heat required for anti-tumor therapy. Furthermore, HIFU is regarded as a highly effective therapeutic tool when combined with nanoparticles enhancing biologically beneficial energy generation on the legion [40]. In particular, the combination of gold nanoparticles with HIFU technology for therapeutic applications has been thoroughly investigated [41] and HIFU can focus directly onto the tumor below the surface of the skin and generate energy.

When tumor reached a volume of 100 mm^3, mice were divided into six groups: (a) saline, (b) saline + laser, (C) saline + HIFU, (d) PEI/RNAi-AuNP, (e) PEI/RNAi-AuNP + laser, and (f) PEI/RNAi-AuNP + HIFU (*n* = 4 per each group). To normalize the tumor vascular environment and consequently hinder tumor growth, first PEI/RNAi-AuNP was administered into solid tumors at the initial stages of PC-3 tumor progression (days 3, 6 and 9). Laser or HIFU irradiation was then performed to ablate tumors when tumors began to grow faster (days 12, 14 and 16) (Fig. 7a). In the initial tumor growth stage up to 12 days, the tumors treated with PEI/RNAi-AuNP exhibited relatively low growth rate compared to other experimental groups without PEI/RNAi-AuNP (Fig. 7b,c). Anti-angiogenesis therapy with anti-VEGF siRNA to reduce tumor growth was performed at early tumor development stages and we could clearly observe the statistically significant tumor suppression effect resulted from the VEGF gene silencing of PEI/RNAi-AuNP for up to 12 days in Fig. 7b. Finally, for anti-VEGF siRNA monotherapy alone (PEI/RNAi-AuNP), as expected the tumors began to regrow within 3 days after the last PEI/RNAi-AuNP treatment and had finally reached similar sizes to the control groups at later stages of tumor progression.

On the contrary, the tumors with laser or HIFU irradiation were completely eradicated under the same experimental conditions as used for anti-VEGF siRNA monotherapy. The hind flank tumor images on day 12 and 16 clearly revealed small lesions with ulceration as a result of the high amounts of heat generation, causing severe necrosis of tumor cells from laser or HIFU irradiation (Fig. 7d). The ulcer wounds were fully healed for all mice exposed to PEI/RNAi-AuNP with laser or HIFU irradiation within 2 weeks' post-treatment.

In order to examine the effect of the combination therapy in detail, VEGF gene silencing and the extent of vascularization was investigated using the tumors excised on day 16. As shown in Fig. 8, VEGF gene expression was effectively inhibited in terms of VEGF expression level by western blotting analysis (Fig. 8a) and high vascularization and vessel tortuosity were prominently observed in the non-treated groups lacking anti-VEGF siRNA therapy (Fig. 8b). Additionally, the numbers of vessels were significantly reduced for both groups with laser or HIFU treatment compared to that of the non-treated group. Further we observed micro-vessel structures in the control tumor tissues (from Saline injected mice) as well as a few of the tumor micro-vessels in the PEI/RNAi-AuNP + laser/HIFU treated groups in H&E stained tissues at day 30 (indicated by the yellow arrows in Fig. S7).

The therapeutic effects of PEI/RNAi-AuNP with laser or HIFU irradiation were further evaluated in histological examination. The tumor of the control groups treated with saline consisted of intact undamaged PC-3 cancer cells. In contrast, the combination therapy of PEI/RNAi-AuNP with laser or HIFU-induced thermal ablation showed a wide

range of cell death in the tumor tissues, resulting in successful tumor growth inhibition (Fig. 8b). PEI/RNAi-AuNPs were observed as black aggregates within the tumor tissues, and the cancer cells around PEI/RNAi-AuNPs particularly showed heat-induced necrotic changes. These results support that combination of anti-angiogenic and photothermal therapy using PEI/RNAi-AuNP could provide a potential therapeutic strategy for blocking or retarding PC-3 cancer progression.

Conclusion

In summary, a platform technology was established for the construction of highly sophisticated RNA and AuNP hybrid nano-assemblies. Precise synthesis and separation of AuNPs with specific numbers of RNA conjugated to them provided effective building blocks to assemble exquisite nano-assemblies with various geometries. More importantly, the anti-cancer therapeutic potential of RNAi-AuNP was validated *in vitro* and *in vivo* by combining the heat generation capability of AuNPs and VEGF gene silencing activity of siRNA therapeutics. In this study, rational combination of anti-VEGF mechanism for depleting angiogenesis process at initial stage of tumor progression and complete ablation of residual tumors with photothermal activity of AuNPs validated their therapeutic potential in PC-3 xenograft mice.
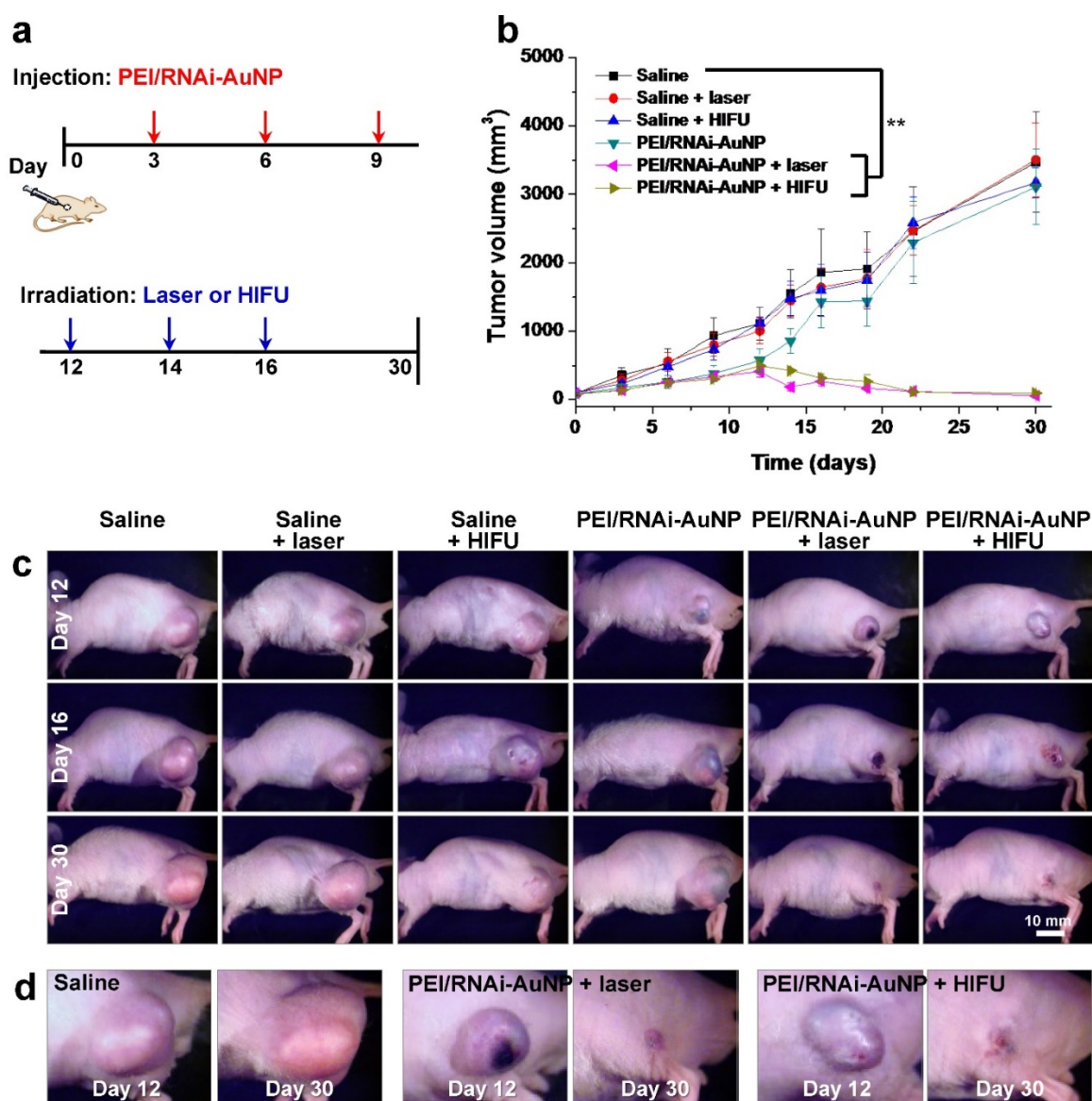
Figure 7. In vivo antitumor therapeutic efficacy with PC-3 tumor bearing mice. (a) Therapeutic regimens for anti-VEGF therapy by siVEGF in combination with photothermal therapy with laser or HIFU. (b) Tumor growth rate graph and (c, d) images at Day 12, 16 and 30 in all tested experimental groups. ** P<0.005 (n=4)
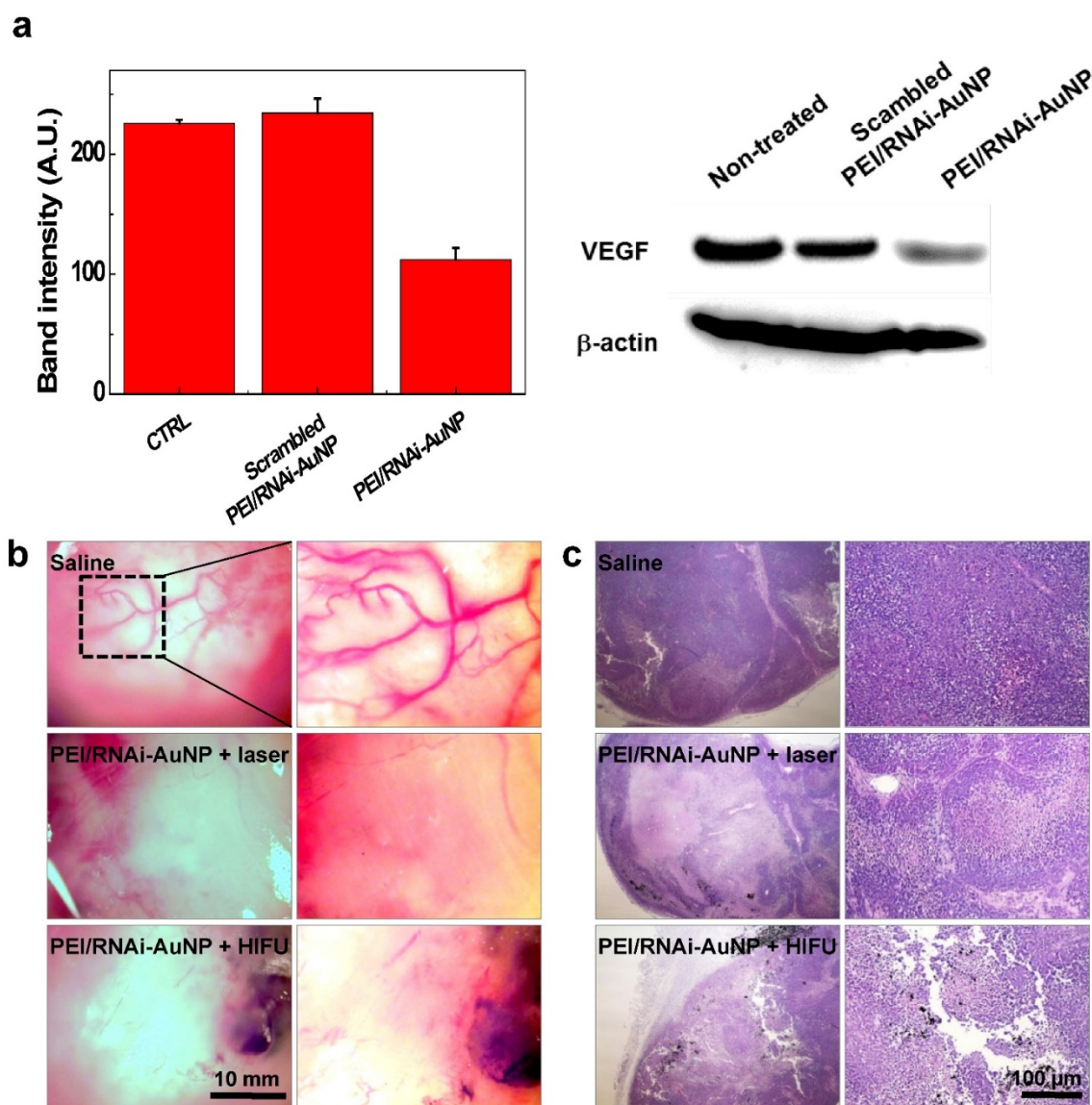
Figure 8. (a) In vivo siVEGF gene silencing efficacy by western blotting analysis of PEI/RNAi-AuNP and scrambled PEI/RNAi-AuNP. (b) Extent of vascularization of solid tumors observed on day 16 after anti-VEGF therapy with PEI/RNAi-AuNP in combination with photothermal therapy with laser or HIFU. (c) Histological examination (H&E staining) of therapeutic efficacy by anti-VEGF and photothermal combination therapy.

Abbreviation

siRNA: small interfering ribonucleic acid; AuNP: gold nanoparticle; VEGF: vascular endothelial growth factor; siVEGF: VEGF siRNA; DNA-AuNP: DNA conjugated AuNP; s-RNA: sense strand of siVEGF; a-RNA: anti-sense strand of siVEGF; RNAi-AuNP: therapeutic siVEGF conjugated AuNP; Poly(RNAi-AuNP): long, linear chain of RNAi-AuNP; PEI/RNAi-AuNP: poly(RNAi-AuNP) complexed with PEI.

Supplementary Material

Supplementary figures.
http://www.thno.org/v07p0009s1.pdf

Competing Interests

The authors have declared that no competing interest exists.

References

1. Seeman NC. DNA in a material world. Nature. 2003; 421: 427-31.
2. Seeman NC. From genes to machines: DNA nanomechanical devices. Trends Biochem Sci. 2005; 30: 119-25.

3. Yatsunyk LA, Mendoza O, Mergny JL. "Nano-oddities": unusual nucleic acid assemblies for DNA-based nanostructures and nanodevices. Accounts of chemical research. 2014; 47: 1836-44.
4. Triberis GP, Dimakogianni M. DNA in the material world: electrical properties and nano-applications. Recent patents on nanotechnology. 2009; 3: 135-53.
5. Xu PF, Noh H, Lee JH, Domaille DW, Nakatsuka MA, Goodwin AP, et al. Imparting the unique properties of DNA into complex material architectures and functions. Mater Today (Kidlington). 2013; 16: 290-6.
6. Opalinska JB, Gewirtz AM. Nucleic-acid therapeutics: basic principles and recent applications. Nat Rev Drug Discov. 2002; 1: 503-14.
7. Yoon HY, Son S, Lee SJ, You DG, Yhee JY, Park JH, et al. Glycol chitosan nanoparticles as specialized cancer therapeutic vehicles: Sequential delivery of doxorubicin and Bcl-2 siRNA. Scientific Reports. 2014; 4: 6878.
8. Son S, Namgung R, Kim J, Singha K, Kim WJ. Bioreducible Polymers for Gene Silencing and Delivery. Accounts of chemical research. 2012; 45: 1100-12.
9. Tiemann K, Rossi JJ. RNAi-based therapeutics-current status, challenges and prospects. EMBO Mol Med. 2009; 1: 142-51.
10. Kole R, Krainer AR, Altman S. RNA therapeutics: beyond RNA interference and antisense oligonucleotides. Nat Rev Drug Discov. 2012; 11: 125-40.
11. Son S, Singha K, Kim WJ. Bioreducible BPEI-SS-PEG-cNGR polymer as a tumor targeted nonviral gene carrier. Biomaterials. 2010; 31: 6344-54.
12. Son S, Kim WJ. Biodegradable nanoparticles modified by branched polyethylenimine for plasmid DNA delivery. Biomaterials. 2010; 31: 133-43.
13. Lee H, Lytton-Jean AK, Chen Y, Love KT, Park AI, Karagiannis ED, et al. Molecularly self-assembled nucleic acid nanoparticles for targeted in vivo siRNA delivery. Nat Nanotechnol. 2012; 7: 389-93.
14. Lee SJ, Huh MS, Lee SY, Min S, Lee S, Koo H, et al. Tumor-homing poly-siRNA/glycol chitosan self-cross-linked nanoparticles for systemic siRNA delivery in cancer treatment. Angew Chem Int Ed Engl. 2012; 51: 7203-7.
15. Son S, Nam J, Kim J, Kim S, Kim WJ. i-motif-driven Au nanomachines in programmed siRNA delivery for gene-silencing and photothermal ablation. ACS Nano. 2014; 8: 5574-84.
16. Elbaz J, Cecconello A, Fan Z, Govorov AO, Willner I. Powering the programmed nanostructure and function of gold nanoparticles with catenated DNA machines. Nat Commun. 2013; 4: 2000.
17. Liu Y, He J, Yang K, Yi C, Liu Y, Nie L, et al. Folding Up of Gold Nanoparticle Strings into Plasmonic Vesicles for Enhanced Photoacoustic Imaging. Angew Chem Int Ed Engl. 2015; 54: 15809-12.
18. Rosi NL, Giljohann DA, Thaxton CS, Lytton-Jean AK, Han MS, Mirkin CA. Oligonucleotide-modified gold nanoparticles for intracellular gene regulation. Science. 2006; 312: 1027-30.
19. Giljohann DA, Seferos DS, Prigodich AE, Patel PC, Mirkin CA. Gene regulation with polyvalent siRNA-nanoparticle conjugates. J Am Chem Soc. 2009; 131: 2072-3.
20. Ding Y, Jiang Z, Saha K, Kim CS, Kim ST, Landis RF, et al. Gold nanoparticles for nucleic acid delivery. Mol Ther. 2014; 22: 1075-83.
21. Nam J, Won N, Jin H, Chung H, Kim S. pH-Induced aggregation of gold nanoparticles for photothermal cancer therapy. J Am Chem Soc. 2009; 131: 13639-45.
22. Kim J, Lee YM, Kang Y, Kim WJ. Tumor-homing, size-tunable clustered nanoparticles for anticancer therapeutics. ACS Nano. 2014; 8: 9358-67.
23. Poletti A, Fracasso G, Conti G, Pilot R, Amendola V. Laser generated gold nanocorals with broadband plasmon absorption for photothermal applications. Nanoscale. 2015; 7: 13702-14.
24. Choi SW, Makita N, Inoue S, Lesoil C, Yamayoshi A, Kano A, et al. Cationic comb-type copolymers for boosting DNA-fueled nanomachines. Nano Lett. 2007; 7: 172-8.
25. Chen L, Di J, Cao C, Zhao Y, Ma Y, Luo J, et al. A pH-driven DNA nanoswitch for responsive controlled release. Chem Commun (Camb). 2011; 47: 2850-2.
26. Zanchet D, Micheel CM, Parak WJ, Gerion D, Williams SC, Alivisatos AP. Electrophoretic and Structural Studies of DNA-Directed Au Nanoparticle Groupings. The Journal of Physical Chemistry B. 2002; 106: 11758-63.
27. Zanchet D, Micheel CM, Parak WJ, Gerion D, Alivisatos AP. Electrophoretic Isolation of Discrete Au Nanocrystal/DNA Conjugates. Nano Letters. 2001; 1: 32-5.
28. Pei H, Li F, Wan Y, Wei M, Liu H, Su Y, et al. Designed Diblock Oligonucleotide for the Synthesis of Spatially Isolated and Highly Hybridizable Functionalization of DNA–Gold Nanoparticle Nanoconjugates. Journal of the American Chemical Society. 2012; 134: 11876-9.
29. Snyder TM, Tse BN, Liu DR. Effects of template sequence and secondary structure on DNA-templated reactivity. J Am Chem Soc. 2008; 130: 1392-401.
30. Brown KA, Park S, Hamad-Schifferli K. Nucleotide−Surface Interactions in DNA-Modified Au−Nanoparticle Conjugates: Sequence Effects on Reactivity and Hybridization. The Journal of Physical Chemistry C. 2008; 112: 7517-21.
31. Aldaye FA, Sleiman HF. Dynamic DNA templates for discrete gold nanoparticle assemblies: control of geometry, modularity, write/erase and structural switching. J Am Chem Soc. 2007; 129: 4130-1.
32. Verma A, Stellacci F. Effect of surface properties on nanoparticle-cell interactions. Small. 2010; 6: 12-21.
33. Akinc A, Thomas M, Klibanov AM, Langer R. Exploring polyethylenimine-mediated DNA transfection and the proton sponge hypothesis. J Gene Med. 2005; 7: 657-63.
34. Benjaminsen RV, Mattebjerg MA, Henriksen JR, Moghimi SM, Andresen TL. The possible "proton sponge " effect of polyethylenimine (PEI) does not include change in lysosomal pH. Mol Ther. 2013; 21: 149-57.
35. Prager GW, Poettler M, Unseld M, Zielinski CC. Angiogenesis in cancer: Anti-VEGF escape mechanisms. Transl Lung Cancer Res. 2012; 1: 14-25.
36. Jain RK, Duda DG, Clark JW, Loeffler JS. Lessons from phase III clinical trials on anti-VEGF therapy for cancer. Nat Clin Pract Oncol. 2006; 3: 24-40.
37. Day ES, Zhang L, Thompson PA, Zawaski JA, Kaffes CC, Gaber MW, et al. Vascular-targeted photothermal therapy of an orthotopic murine glioma model. Nanomedicine (Lond). 2012; 7: 1133-48.
38. Markman JL, Rekechenetskiy A, Holler E, Ljubimova JY. Nanomedicine therapeutic approaches to overcome cancer drug resistance. Adv Drug Deliv Rev. 2013; 65: 1866-79.
39. Son S, Min HS, You DG, Kim BS, Kwon IC. Echogenic nanoparticles for ultrasound technologies: Evolution from diagnostic imaging modality to multimodal theranostic agent. Nano Today. 2014; 9: 525-40.
40. You DG, Deepagan VG, Um W, Jeon S, Son S, Chang H, et al. ROS-generating TiO2 nanoparticles for non-invasive sonodynamic therapy of cancer. Sci Rep. 2016; 6: 23200.
41. Wang X, Chen H, Zheng Y, Ma M, Chen Y, Zhang K, et al. Au-nanoparticle coated mesoporous silica nanocapsule-based multifunctional platform for ultrasound mediated imaging, cytoclasis and tumor ablation. Biomaterials. 2013; 34: 2057-68.